[Geophysical Research Letters]

Supporting Information for

A Deep Learning Approach to Extract Balanced Motions from Sea Surface Height Snapshot

Zhanwen Gao[1,2], Bertrand Chapron[2], Chunyong Ma[1,3], Ronan Fablet[4], Quentin Febvre[4], Wenxia Zhao[1], Ge Chen[1,3]

[1]Department of Marine Technology, Ocean University of China, Qingdao, China

[2]Ifremer, UMR CNRS LOPS, Brest, France

[3]Laoshan Laboratory, Qingdao, China

[4]IMT Atlantique, UMR CNRS Lab-STICC, Brest, France

Corresponding author: Chunyong Ma (chunyongma@ouc.edu.cn)

Ge Chen (gechen@ouc.edu.cn)

Contents of this file

Introduction

This supporting information includes the global location of the experimental regions selected in this study (Text S1), the detailed calculation process of the azimuthally-averaged methodology (Text S2), the decomposition of the balanced motions (BM) and unbalanced motions (UBM) for the sea surface velocity data (Text S3), the correlation and wavenumber-frequency spectrum diagnosis (Text S4), and the seasonality of the BM and UBM (Text S5). Eight supporting figures are included in this document that support either the information presented in this document or the main text.

Text S1. Global Location of the Experimental Regions in this Study

Two 5°×5° areas are selected as the experimental regions in this study, including the Gulf Stream (38°-43°N, 60°-65°W) and South China Sea (17.5°-22.5°N, 115°-120°E), as shown by the blue boxes in the enlarged images at the bottom (Figure S1).

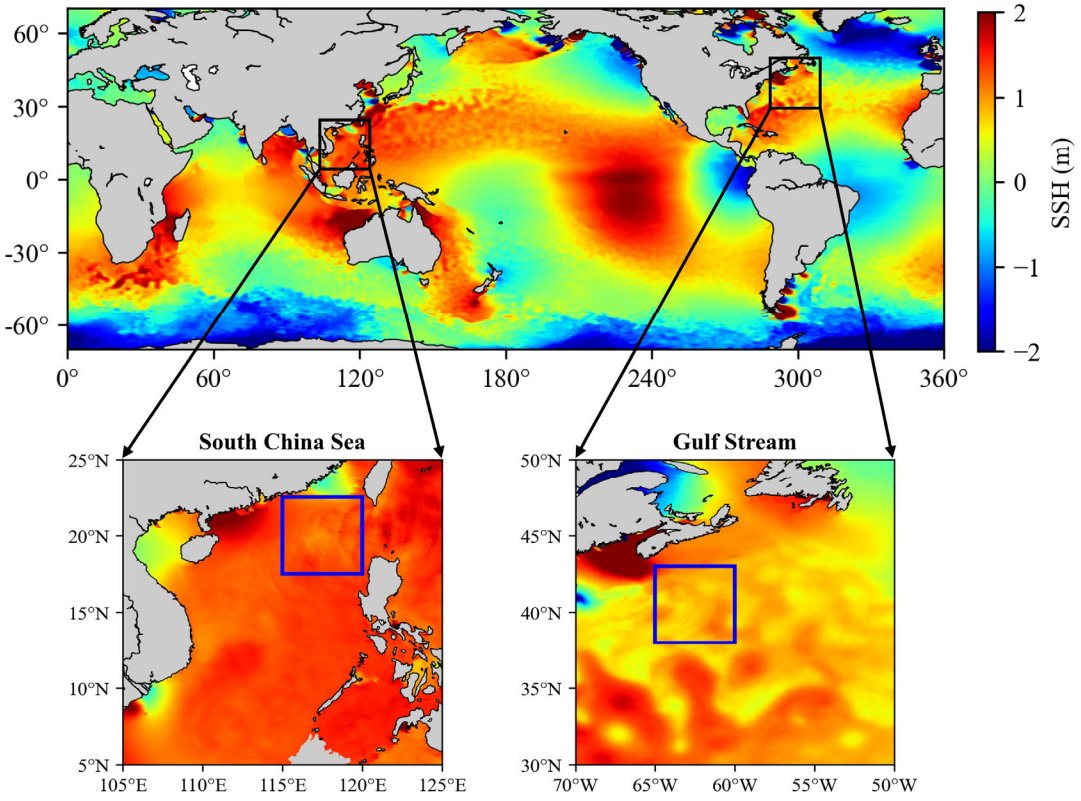

Figure S1. Experimental regions selected in this study (blue boxes at the bottom): Gulf Stream and South China Sea.

Text S2. Detailed Calculation Process of the Azimuthally-Averaged Methodology

The two-dimensional (2D) wavenumber spectrum $\hat{T}(k,l)$ corresponding to the 2D scalar $T(x,y)$ is obtained by performing a 2D Fourier transform, where k and l are the zonal wavenumber and meridional wavenumber, respectively. The power spectral density (PSD) is calculated by:

$$S(k,l) = \left|\hat{T}(k,l)\right|^2 * \frac{dxdy}{N_x N_y} \tag{1}$$

where dx and dy are the distances between adjacent grid points in the zonal and meridional directions, and N_x and N_y are the numbers of grid points in the zonal and meridional directions, respectively.

Then, we employ the azimuthally-averaged methodology to transform the 2D isotropic spectrum into the 1D spectrum. Specifically, it converts the 2D spectrum from the Cartesian coordinate to the polar coordinate. If we define $k_r^2 = k^2 + l^2$, then the sum of the PSD in these two coordinates can be expressed as:

$$\int_{-l_{max}}^{l_{max}} \int_{-k_{max}}^{k_{max}} S(k,l)dkdl = \int_0^{k_{r_{max}}} \int_{-\pi}^{\pi} S(k_r,\theta)k_r d\theta dk_r \tag{2}$$

where $k_{max} = 1/(2dx)$, $l_{max} = 1/(2dy)$, $k_{r_{max}} = \max(k_{max}, l_{max})$. The 1D spectrum can be obtained through the integration with respect to θ:

$$S(k_r) = \int_{-\pi}^{\pi} S(k_r,\theta)k_r d\theta \tag{3}$$

Taking a fixed point $k_r = k_{r0}$ as an example, $S(k_{r0})$ is obtained by calculating the average value of multiple PSD values in the 2D spectrum.

$$S(k_{r0}) = \int_{-\pi}^{\pi} S(k_{r0},\theta)k_{r0} d\theta = \frac{2\pi \sum_{i=1}^{n} k_r S(k,l)}{n} \tag{4}$$

n is the number of PSD values participating in the calculation of the average value, which must satisfy the following relationship:

$$\left(k_{r0} - \frac{\Delta k_r}{2}\right)^2 < k^2 + l^2 < \left(k_{r0} + \frac{\Delta k_r}{2}\right)^2 \tag{5}$$

$$\Delta k_r^2 = \Delta k^2 + \Delta l^2 \tag{6}$$

Text S3. BM-UBM Decomposition for the Sea Surface Velocity

We use the same dynamically based decomposition methodology to separate the BM and UBM from the sea surface velocity data, which relies on analyzing the spectral differences between these two motions in the kinetic energy (KE) wavenumber-frequency spectrum (Qiu et al., 2018). The delimiting frequencies used are the local tenth vertical-mode inertia–gravity waves (IGWs) dispersion curve, as shown by the red line in Figure S2h. Figure S2a-S2b display the zonal component (U) and meridional component (V) of the sea surface velocity, respectively. Following the decomposition process, Figure S2c-S2d are U and V components corresponding to the BM, and Figure S2e-S2f are U and V components corresponding to the UBM, respectively. The BM clearly exhibits large-scale current velocity signals, whereas the UBM contains abundant velocity information at smaller scale. We also calculate the KE wavenumber spectra for the BM and UBM, as shown in Figure S2g. The BM has higher energy at large scales and its spectral slope is generally k^{-3}, which is consistent with the inference of the interior quasi-geostrophic (QG) turbulence theory (Charney et al., 1971). The UBM dominants at submesoscale ranges with the shallower wavenumber spectrum approximately following k^{-2} power law, consistent with the researches of Rocha et al. (2016) and Chereskin et al. (2019).

The relative vorticity ($\zeta = \frac{\partial v}{\partial x} - \frac{\partial u}{\partial y}$) and horizontal divergence ($\delta = \frac{\partial u}{\partial x} + \frac{\partial v}{\partial y}$) are calculated for the total sea surface velocity, the BM components and the UBM components. For the relative vorticity (Figure S3c and S3e), mesoscale geostrophic features present in the BM components, while IGWs footprints clearly exhibit in the UBM. Regarding the horizontal divergence (Figure S3d and S3f), the UBM accounts for most of the total horizontal divergence, while it is extremely small in the BM. Nevertheless, the BM still contains a small fraction of the horizontal divergence, primarily originating from submesoscale motions. And this result also reminds us to be more cautious when using the Helmholtz decomposition, which assumes that the BM is nondivergent and the total divergence is due to the UBM. Torres et al. (2018) also discussed the limitations of the Helmholtz decomposition.

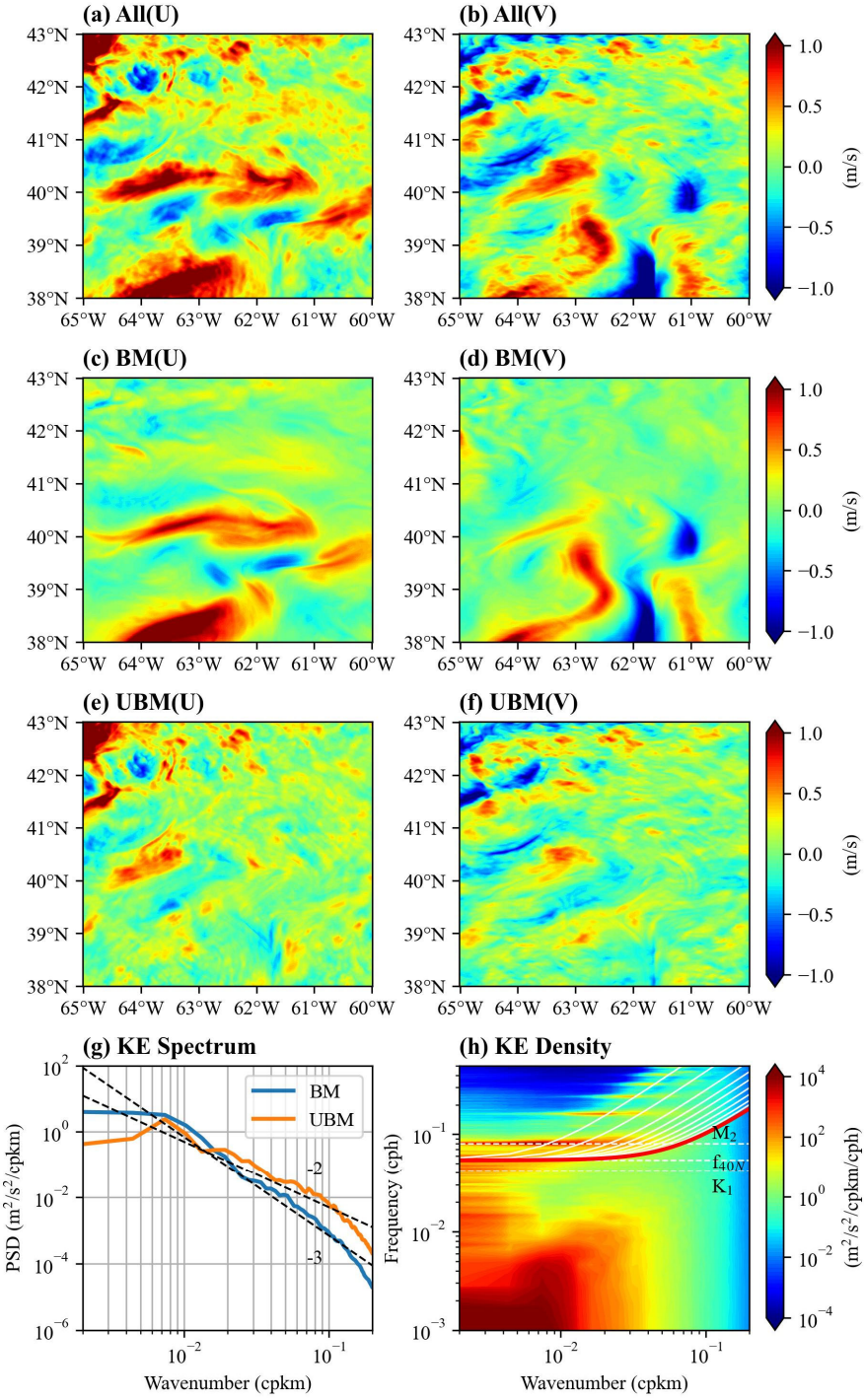

Figure S2. The BM-UBM decomposition results for the sea surface velocity. (a) and (b) are the zonal component (U) and meridional component (V) of the sea surface velocity. (c)-(f) are the decomposition results of U and V components corresponding to the BM and UBM. (g) is the wavenumber spectrum of the BM and UBM, where black dashed lines denote spectral slopes of k^{-2} and k^{-3} for reference. (h) is the KE wavenumber-frequency spectrum. Dashed white lines denote the inertial and tidal frequencies. Solid white lines denote the dispersion relation for IGWs of the first 10 vertical modes. Solid red line denotes the dynamic frequencies to separate the BM and UBM.

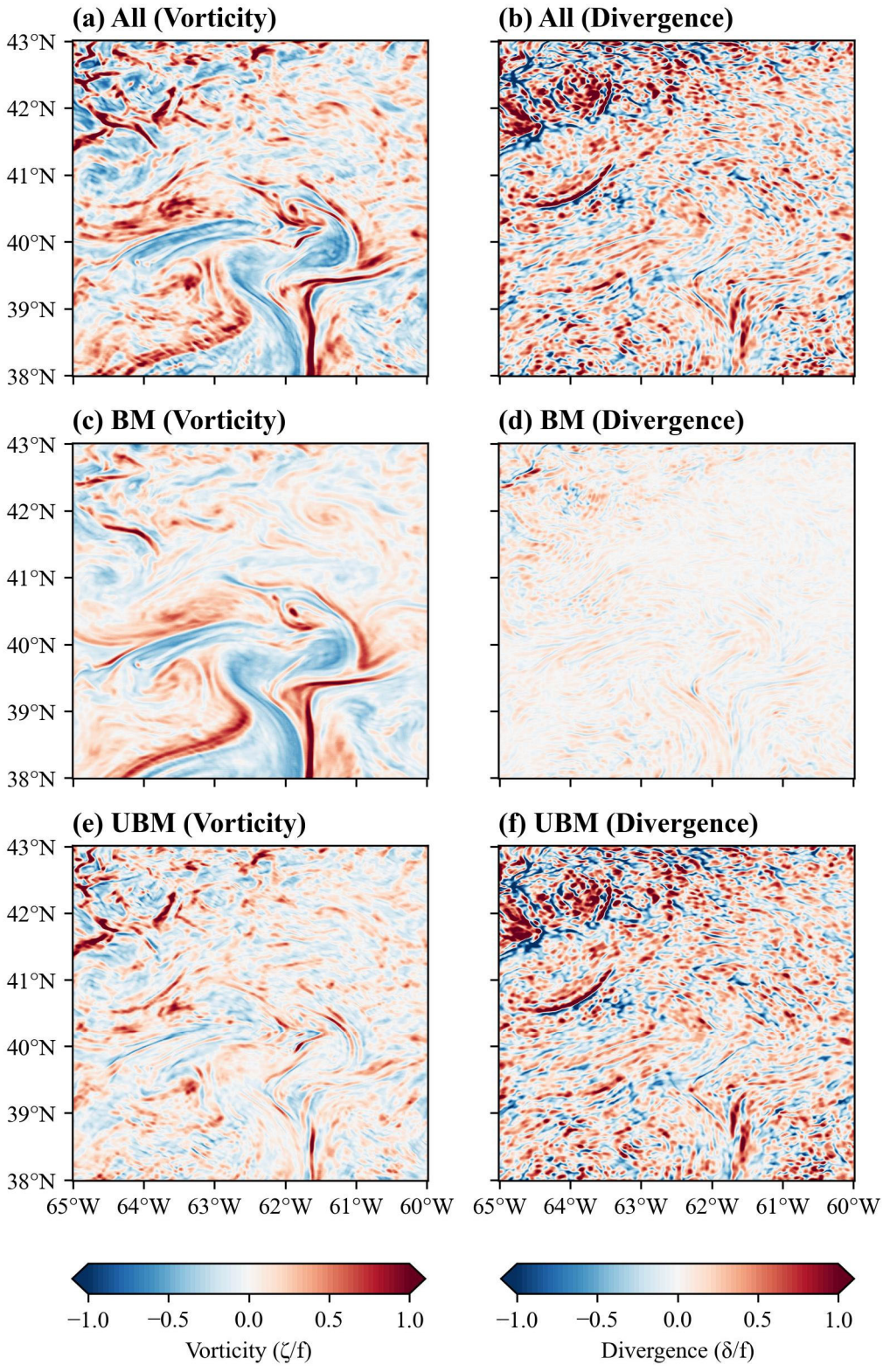

Figure S3. The relative vorticity and horizontal divergence (both divided by the planetary vorticity f) calculated for the total sea surface velocity, the BM components and the UBM components.

Text S4. Correlation and Wavenumber-Frequency Spectrum Diagnosis

Figure S4 and Figure S6 plot the correlation between the BM (True) and BM (DL). A total of 240 SSH snapshots are tested, and results show that the average correlation coefficients are 0.996 and 0.97 in the Gulf Stream and the South China Sea, respectively.

The third metric, wavenumber-frequency spectrum, to further evaluate the capability of the BM-UBM Network. The wavenumber-frequency spectra of the BM, UBM, error and the ratio of error with both signals are plotted in Figure S5 and Figure S7. The predicted UBM obtained from the BM-UBM Network can well describe the dispersion relation for IGWs of different modes (Figure S5d and Figure S7d). And the signal-to-noise ratio (SNR) of the BM and UBM respectively shows that SNR values greater than 1 are concentrated in the low-frequency regions dominated by the BM (Figure S5c and Figure S7c) and the high-frequency regions dominated by the UBM (Figure S5e and Figure S7e).

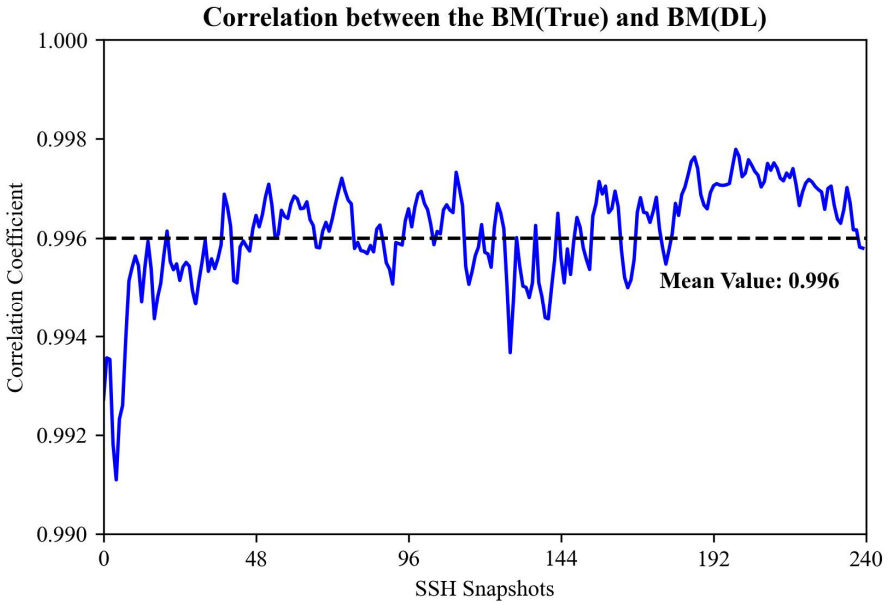

Figure S4. Correlation between the BM from ground truth and BM from deep learning approach in the Gulf Stream. The black dashed line represents the mean value of correlation coefficient.

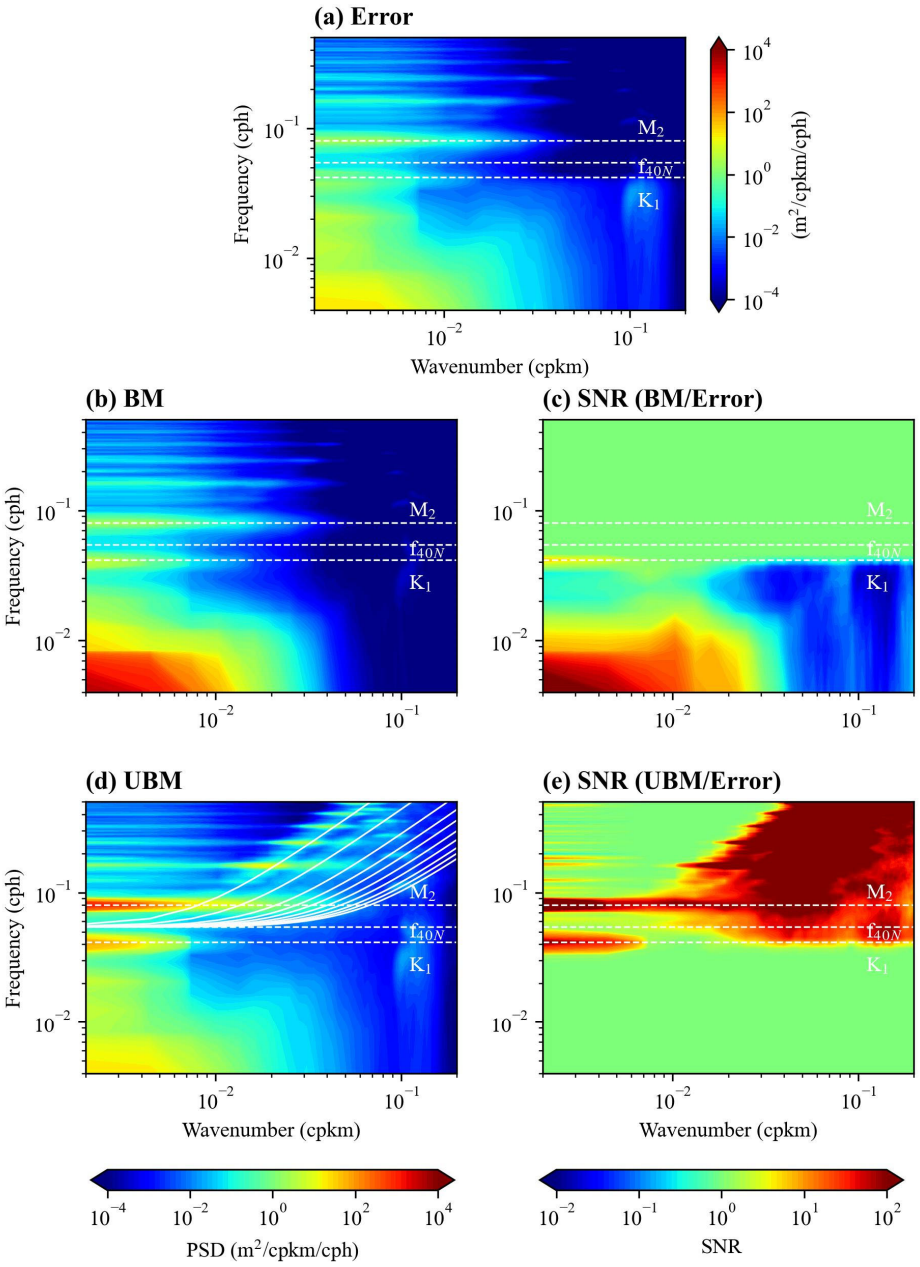

Figure S5. The wavenumber-frequency spectra of the (a) Error, (b) BM, (d) UBM over the testing dataset in the Gulf Stream. (c) and (e) are the SNR of the BM and UBM, respectively.

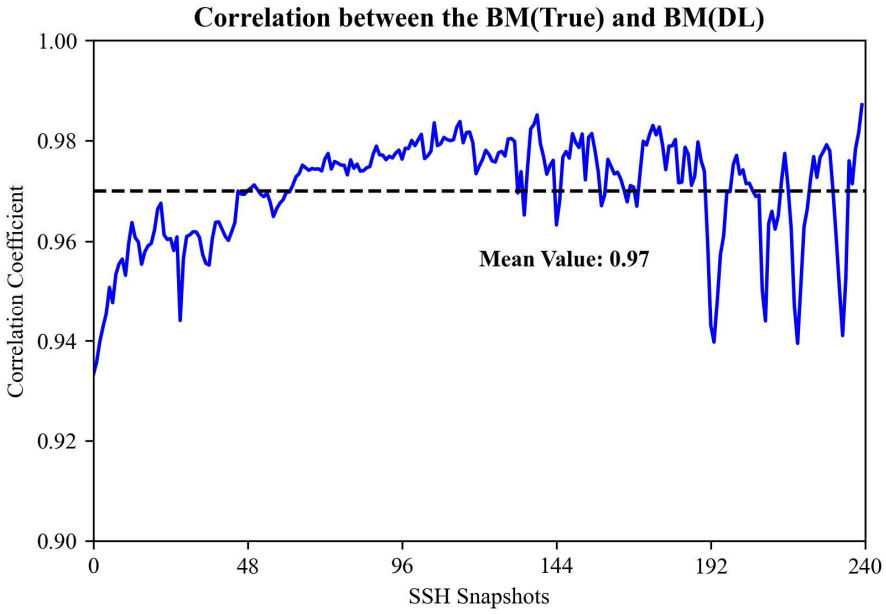

Figure S6. Correlation between the BM from ground truth and BM from deep learning approach in the South China Sea. The black dashed line represents the mean value of correlation coefficient.

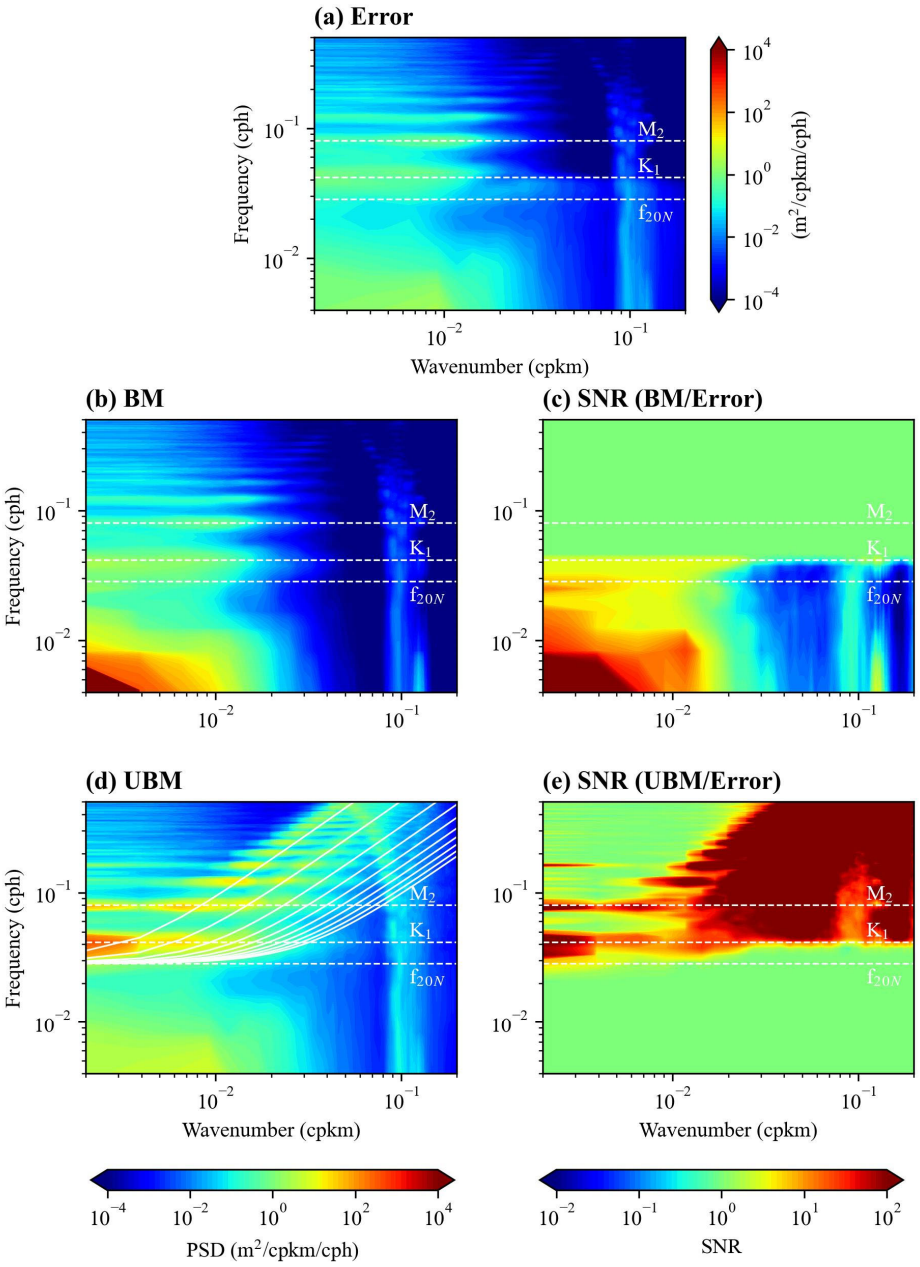

Figure S7. The wavenumber-frequency spectra of the (a) Error, (b) BM, (d) UBM over the testing dataset in the South China Sea. (c) and (e) are the SNR of the BM and UBM, respectively.

Text S5. Seasonality of the BM and UBM

Based on sea surface velocity data of MITgcm llc4320, we compute the relative vorticity and horizontal divergence on two specific dates. It is found that there are larger values and fine-grained relative vorticity pattern on the March 1, 2012, and the root-mean-square (RMS) of the relative vorticity is about $0.45f$ (f is the local planetary vorticity). While the situation is the opposite on the September 1, 2012, which has a relatively coarse-grained pattern and smaller values of the relative vorticity ($0.29f$ of RMS). However, the RMS of horizontal divergence is about $0.48f$ on September 1, which is relatively larger compared to the $0.27f$ on March 1. Rocha et al. (2016) argued that this phenomenon is attributed to vigorous out-of-phase seasonal cycles of the BM and UBM, where the BM dominates the horizontal velocity in late winter/early spring, while the UBM dominates the horizontal velocity in late summer/early autumn.

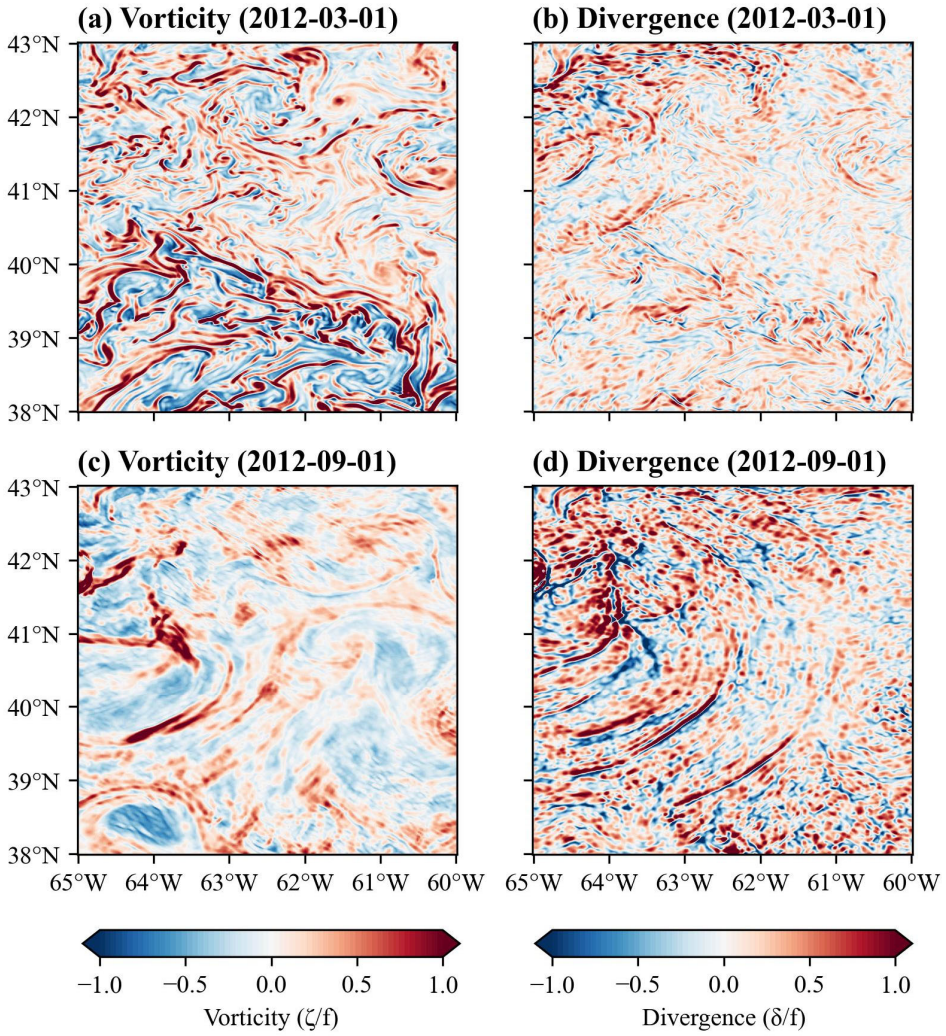

Figure S8. The relative vorticity and horizontal divergence (both divided by the planetary vorticity f) calculated for the sea surface velocity from MITgcm llc4320 dataset. (a) and (b) correspond to March 1, 2012, (c) and (d) correspond to September 1, 2012.

Reference

Charney, J. G. (1971). Geostrophic turbulence. *Journal of the Atmospheric Sciences*, 28(6), 1087-1095. https://doi.org/10.1175/1520-0469(1971)028<1087:GT>2.0.CO;2

Chereskin, T. K., Rocha, C. B., Gille, S. T., Menemenlis, D., & Passaro, M. (2019). Characterizing the transition from balanced to unbalanced motions in the southern California Current. *Journal of Geophysical Research: Oceans*, 124, 2088–2109. https://doi.org/10.1029/2018JC014583

Qiu, B., Chen, S., Klein, P., Wang, J., Torres, H., Fu, L.-L., & Menemenlis, D. (2018). Seasonality in transition scale from balanced tounbalanced motions in the world ocean. *Journal of Physical Oceanography*, 48, 591–605. https://doi.org/10.1175/JPO-D-17-0169.1

Rocha, C. B., Gille, S. T., Chereskin, T. K., & Menemenlis, D. (2016). Seasonality of submesoscale dynamics in the Kuroshio Extension. *Geophysical Research Letters*, 43, 11,304–11,311. https://doi.org/10.1002/2016GL071349

Torres, H. S., Klein, P., Menemenlis, D., Qiu, B., Su, Z., Wang, J., et al. (2018). Partitioning ocean motions into balanced motions and internal gravity waves: A modelling study in anticipation of future space missions. *Journal of Geophysical Research: Oceans*, 123, 8084–8105. https://doi.org/10.1029/2018JC014438